High energy density of primary lithium batteries working with sub-fluorinated few walled carbon nanotubes cathode

Yasser Ahmad, Marc Dubois, Katia Guérin, André Hamwi, Emmanuel Flahaut

High energy density of primary lithium batteries working with sub-fluorinated few walled carbon nanotubes cathode

Yasser Ahmad [a], Marc Dubois [a], Katia Guerin [a, *], André Hamwi [a], Emmanuel Flahaut [b, c]

[a] Université Clermont Auvergne, CNRS, SIGMA Clermont, Institut de Chimie de Clermont-Ferrand, F-63000, Clermont–Ferrand, France
[b] Université de Toulouse, UPS, INSA, INP, ISAE, LAAS, F-31059, France
[c] Université de Toulouse, UPS, INP, Institut Carnot Cirimat, F-31062, Toulouse, France

A B S T R A C T

Fluorinated carbon nanotubes used as cathode material exhibit a capacity exceeding the theoretical value when used in primary lithium battery. The measured experimental capacity, the faradic yield and the energy density were increased, exceeding the expected theoretical values for sub-fluorinated few walled carbon nanotubes (FWCNTs).Although the molar carbon/fluorine ratio was only of 0.37 (i.e $CF_{0.37}$), an experimental capacity of 900 mAh.g^{-1} was obtained which is higher than the theoretical value of 521 mAh.g^{-1}. With the same material, an unprecedented energy density of 2565 Wh kg^{-1} was reached associated with a faradic yield of 172%. The materials were deeply characterized using TEM, Raman and solid state ^{13}C and ^{19}F NMR in order to explain the extra-capacity. Such high electrochemical values can be correlated to the reinforcement effect of the central tube(s), coupled with a low amount of structural defects.

Keywords:
Fluorinated carbon nanotubes
Cathode
Lithium battery
Energy density
Extra-capacity
Reinforcement effect

1. Introduction

Fluorinated carbons (CF_x) are used as cathode material in primary lithium batteries (Li/CF_x) since the 70's [1,2] because high oxidation-reduction potential of the cathode reaction is combined with low weight densities of light carbon and fluorine elements. Due to the target applications such as cameras, electrical locks, electronic counters, electronic measurement equipment, emergency power sources, memory back-ups, spatial, military fields and implantable medical devices, power sources with high energy densities, good reliability, safety and long life are required. Commercial Li/CF_x batteries working with a coke based cathode and having a F/C molar ratio equal or slightly higher than 1 exhibit many advantages, i.e. high energy density (up to 1560 Wh kg^{-1}), high average operating voltage (around 2.4 V vs. Li$^+$/Li), long shelf-life (higher than 10 years at room temperature), stable operation and a wide operating temperatures range (−40 °C/170 °C). However they have some drawbacks such as low power density (around 1400 W kg^{-1}) and low faradic yield (not more than 75% because of too high amounts of inactive CF_2 and CF_3 groups and dangling bonds which are considered as structural defects hindering the lithium diffusion) [3]. Researches have recently focused on minimizing those drawbacks especially concerning the power density. The enhancement of the extrinsic or intrinsic electrical conductivity of CF_x cathode materials was a way to achieve such a goal. Some carbon atoms may be excluded for the fluorination in order to keep conductive parts inside the insulating fluorinated carbonaceous lattice; the concept was called “sub-fluorination”. The electron flux in the electrode is then ensured through these conductive paths. The first reported work concerned fluorinated carbon nanofibers; an impressive 8057 W kg^{-1} power density associated with a high 1749 Wh kg^{-1} energy density were achieved [4,5]. Going further on this strategy, Yue et al. [6] have found that fluorinated carbon nanotubes with F/C ratio of 0.75 exhibited the best energy and power densities never reported, i.e. 1147 Wh kg^{-1} and 8998 W kg^{-1}, respectively, at a current density of 4 A g^{-1}. For this case also, the explanations of the good performances are related to fluorine atoms dispersion: fluorine atoms were located at the outer part of the carbon nanotubes where graphene layers were initially coaxial within a distance of 0.60 nm. In contrast, the inner part of the carbon nanotubes remained unchanged. A conductive component may be added on the surface of the CFx material for example

* Corresponding author. CNRS, UMR 6296, Institut de Chimie de Clermont-Ferrand, F-63170, Aubiere, France.
E-mail address: katia.araujo_da_silva@uca.fr (K. Guerin).

by electrodeposition of polypyrrole (PPy) onto graphite fluorides ($CF_{0.80}$) (in acetonitrile containing Pyrrole monomer) [7]. Those examples highlight that the fluorine content, or F/C ratio, may be decreased keeping the capacity high. On the other hand, enhancements of the energy densities were achieved mainly by an increase in the discharge potential [8,9]. The capacity has been considered as limited to a theoretical value 864 mAh.g^{-1} for a maximal CF_1 composition. Nevertheless, capacity increase beyond this limit goes through the deep understanding of the discharge mechanism. It is admitted that the products after the electrochemical defluorination are amorphous carbon and LiF. A graphite intercalation compound (GIC) intermediate with solvated lithium is formed on the graphite sheets edges and acts as a diffusion layer [10]. Moreover, the concentration of lithium ions decreases rapidly with the distance from the electrode surface meaning that lithium ions stay out of the fluorocarbon matrix. On sheet edges, the GIC subsequently decomposes into the final discharge products, carbon and LiF. The discharge is accompanied by significant electrode swelling due to the formation of volumetric LiF crystals as reported by Abraham et al. [11]. Based on the discharge and OCV recovery characteristics, Zhang et al. [12] proposed a discharge through a "shrinking core" model consisting of a CFx core and a product shell. This latter is composed of intermediate GIC, carbon and lithium fluoride. The product shell grows with the discharge process, and its composition varies with the decomposition of intermediate GIC.

A recent work appears as a breakthrough technology [13]: when a part of the carbon lattice, namely the central discs, less or not fluorinated, acts as a reinforcement, the rebuilding of the carbonaceous lattice during the electrochemical discharge forms a new host matrix which is covered with LiF shell. An additional lithium insertion could occur in the newly formed carbon structure by the electrochemical de-fluorination. Extra-capacities up to 1180 mAh.g^{-1} were then obtained in Li/CFx primary lithium battery using fluorinated carbon nanodiscs as cathode material with 1 M $LiClO_4$ propylene carbonate electrolyte (whereas the theoretical value was 847 mAh.g^{-1} for $CF_{0.95}$ composition). The same phenomenon is expected to occur in different nanostructured carbonaceous materials where the central parts (discs, tubes, core for 2D, 1D and 0D aspects, respectively) may act in the same manner, i.e. reinforcement during the electrochemical defluorination. Moreover, the diffusion length of both Li^+ and F^- must be shortened in order to achieve efficient diffusion of F^-/Li^+ions during defluorination and insertion, respectively. Among the various allotropic forms of carbon, we focus on 1D carbon nanotubes where the inner tube(s) may act as reinforcement. Both criteria, reinforcement and short ions diffusion length, are satisfied a priori. Double-, few- and multi-walled carbon nanotubes were thus investigated in this work. The fluorination processes were optimized to keep the inner tube non-fluorinated and the resulting materials deeply characterized before the electrochemical investigations.

2. Experimental

2.1. Carbon nanotubes CNTs

In order to cover different outer diameters and numbers of walls, several research grade and commercialy available carbon nanotubes have been selected.

Double walled carbon nanotubes (DWCNTs) with high purity (95% of carbon) were synthesized by chemical catalytic vapor deposition (CCVD at 1000 °C), with CoMo-MgO as catalyst [14]. They consist of 90% of DWCNT having an average diameter of ~2 nm and consisting of 2 walls, and contain some disorganized carbon [15]. No further annealing step was applied.

Few walled carbon nanotubes (FWCNTs) with high purity (90% of carbon) were supplied by Helix Corporation. The 10% impurities are amorphous carbon. They were obtained by chemical vapor deposition (CVD) and thermally treated at 1800 °C in an argon atmosphere to enhance their graphitization degree. They consist of tubes having a diameter of ~4 nm [16] with few walls (5–10 walls).

Carbon nanofibers (CNFs) with high purity (90% of carbon), 2–20 μm in length, were supplied by MER Corporation, Tucson, Arizona. They were obtained by CVD and thermally treated at 1800 °C in an argon atmosphere to enhance their graphitization degree. They are considered as multi walled carbon nanotubes (MWCNTs) with about 35 walls without well-defined core and consisted of tubes having a diameter of 140 ± 30 nm.

Differences in the number of walls and structural order result in different fluorination conditions which must be optimized in order to reach similar fluorine content, i.e. molar ratio F/C or x in CFx (x = F/C).

2.2. Fluorination conditions

A passivated nickel reactor was used (passivated with NiF_2) and nitrogen outgassing was applied before and after each fluorination experiment. Fluorinated carbon nanotubes (DWCNTs and FWCNTs) and nanofibres (denoted CNFs) were prepared using dynamic fluorination with a flux of pure molecular fluorine F_2. Gaseous fluorine was purchased from Solvay Fluor (purity 98–99% V/V with HF max. 0.5% V/V and other gases, primarily O_2/N_2 at approximately 0.5% V/V).

In this process, 200 mg of CNTs (DWCNTs, FWCNTs or CNFs) were placed under a pure fluorine gas flow (1 atm) at fluorination temperatures T_F ranging between 300 °C and 350 °C and for a reaction time of 3 h. The resulting samples are denoted **DW-300**,, DW for DWCNTs and **FW-350** for FWCNTs; CNFs were treated at T_F equal to 405 °C; the resulting sample is denoted as **CNF-405.**

The F/C molar ratio of the samples was determined by weight uptake and quantitative ^{19}F NMR. More details about fluorination mechanisms can be found elsewhere [8,17–21]. The fluorination conditions were optimized in order to obtain a similar F/C ratio of 0.37 for all fluorinated samples.

2.3. Physical-chemical characterizations

The various samples were characterized by Transmission Electron Microscopy TEM (Philips CM200 operating at 200 kV). The nanomaterials were dispersed in ethanol using ultrasonic bath. Few drops of the suspension were deposited onto a copper support grid covered with an ultrathin carbon/formvar films. The grids were subsequently dried at ambient conditions before introduction in the TEM.

NMR experiments were performed with Bruker Avance spectrometer, with working frequencies of 73.4 and 282.2 MHz for ^{13}C and ^{19}F respectively. A magic angle spinning probe (Bruker) operating with a 4 mm rotor was used. For MAS spectra, a simple sequence was performed with a single π/2 pulse length of 4.0 and 3.5 μs for ^{19}F and ^{13}C, respectively. ^{13}C chemical shifts were externally referenced to tetramethylsilane (TMS). ^{19}F chemical shifts were referenced with respect to $CFCl_3$.

Raman spectra were recorded at room temperature using a Jobin Yvon T64000 with a charge coupled device multichannel detector. The radiation source was a 514.5 nm Argon laser line. The laser power was tuned to 10 mW in order not to decompose the material.

2.4. Electrochemical study

The electrochemical performances were investigated using galvanostatic discharges. The electrodes were composed of

fluorinated carbon (about 90% w/w), and polyvinylidene difluoride (PVDF 10% w/w) as binder. After stirring in propylene carbonate (PC), the mixture was spread uniformly onto a stainless steel current collector disk of 10 mm diameter. After the PC evaporation, the electrodes were dried in a vacuum oven at 120 °C overnight to remove traces of water and solvent before their transfer into an argon-filled glovebox. The anode was a lithium metal disk, and the separator was Celgard 2034. A two electrodes cell was used (Swagelok cell type), where lithium was both reference and counter electrodes. The electrolyte was 1.0 M $LiPF_6$ in propylene carbonate/ethylene carbonate/dimethyl carbonate (PC/EC/3DMC; 1:1:3 vol %). The cells were assembled in an argon filled dried glove box. Relaxation was performed for at least 5 h until the open circuit voltage (OCV) stabilization. Galvanostatic discharges, carried out on a VMP2-Z instrument from Biologic, were performed at room temperature by applying a constant current density of 10 mA/g with a cutoff voltage of 2 V. The potential $E_{1/2}$ (V) is the average value extracted from the discharges curve. For each fluorinated sample, 5 cells have been made to ensure the reproducibility and quantify the uncertainties of measure.

3. Results and discussions

3.1. Textural characteristics

Because of the nanostructuration of the carbon nanofibres, and the graphitization post-treatment, the fluorination temperature $\mathbf{T_F}$ was higher than the one needed for graphite in pure 1 atm. F_2 gas. Such nanostructuration needs a progressive fluorination which processes from the outer tubes of the nanofibre toward its core (supported by TEM images). The fluorination mechanism of carbon nanotubes using the direct process has been extensively detailed elsewhere [8].

Double walled carbon nanotubes are an intermediate between SWCNTs and MWCNTs in terms of fluorination conditions. TEM images shown in Fig. 1a allow the quantification of the number of walls of DWCNTs. Most of the tubes exhibit two walls [14].

In the same way, TEM images of the pristine FWCNTs showed that these latter had 5 to 10 nested tubes as evidenced in Fig. 1 b (right-handed side). The high degree of graphitization of the CNFs is evidenced in Fig. 1 c with the presence of perfectly parallel walls for a long distance.

Fluorination conditions (duration, temperature and F_2 gas flow) were drastically controlled in order to fluorinate only outer tube(s), and keep one or more non-fluorinated inner tube(s). Thus, DWCNTs were fluorinated at a fluorination temperature $\mathbf{T_F}$ of 300 °C, while FWCNTs were fluorinated at 350 °C for the same duration (3 h) in order to achieve an equivalent F/C ratio of 0.37 for both. Because of both the much higher number of walls of CNFs and their graphitization post-treatment, $\mathbf{T_F}$ was higher than the one needed for double walled and few walled carbon nanotubes in pure 1 atm. F_2 gas. Thus, CNFs were fluorinated at $\mathbf{T_F} = 405$ °C and the F/C molar ratio was equal to 0.4 ($CF_{0.4}$ composition). One key interest of molecular fluorine F_2 compared to other fluorination routes [8,18,22] is the possibility to modify of only the outer wall(s), which will ensure the electrochemical processes, while retaining the remarkable mechanical and electronic properties of the inner nanotube [14]. In other words, the inner tubes act as reinforcement.

After fluorination, whatever the starting material, the nanotubes preserved their morphology and their tubular shape. The inner tube(s) remained non-fluorinated as evidenced in TEM images (Fig. 2) and by ^{13}C NMR analysis thereafter discussed (Fig. 6). Reinforcing effect is then expected during the electrochemical process in the same way that the central disc in the case of nanodiscs [13].

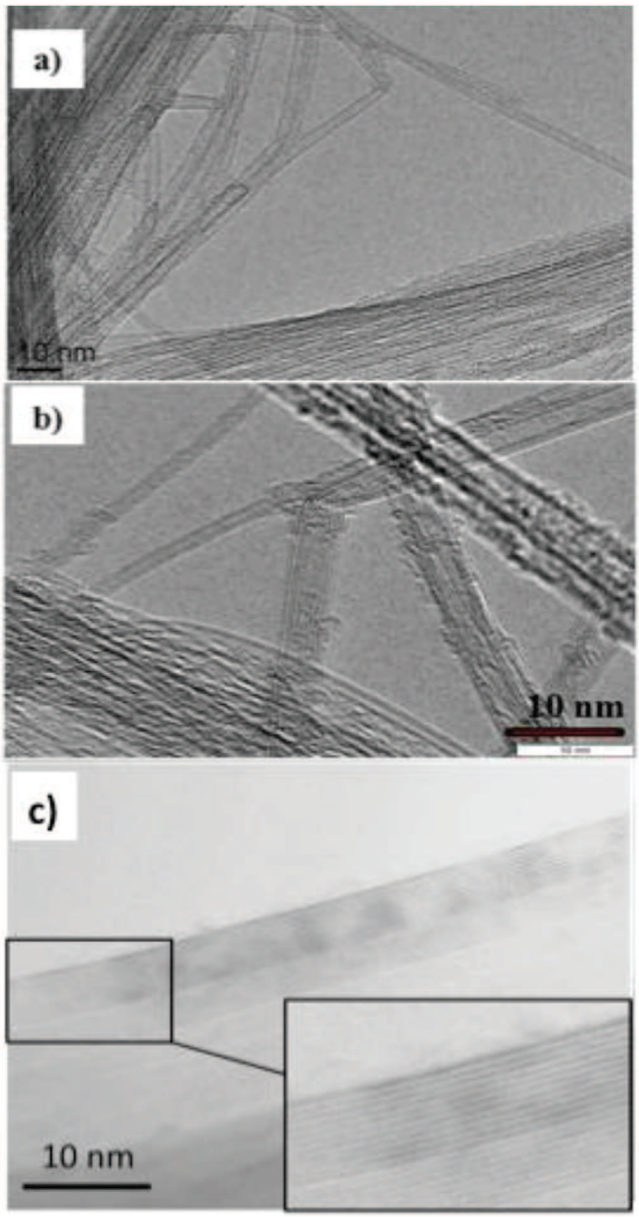

Fig. 1. TEM images of pristine nanotubes DWCNTs (a), FWCNTs (b) and CNFs (c).

3.2. Raman spectroscopy

The Raman spectra of the samples are displayed on Fig. 3. The spectra were recorded in at least 5 different areas of the samples. No difference was found whatever the location. The spectra were normalized to the intensity of the G band. Three narrow vibration bands with full width at half maximum of about 20–40 cm^{-1} are visible: two of them around 1356 and 1620 cm^{-1} are assigned to the **D** and **D′** modes. For their activation **D** and **D′** resonances require a defect, such as bond dislocations, missing atoms at the edges of the sample or sp^3-hybridized carbon atoms; their presence is associated with an increased degree of disorder [23–25]. The third band at 1589 cm^{-1} is assigned to the conventional **G** mode, which is related to the graphitization degree of carbon material and is also called tangential mode (where the carbon atoms in sp^2 hybridization vibrate parallel to the axis of the nanotube) [26].

The D band has a low intensity for DWCNTs, FWCNTs and CNFs

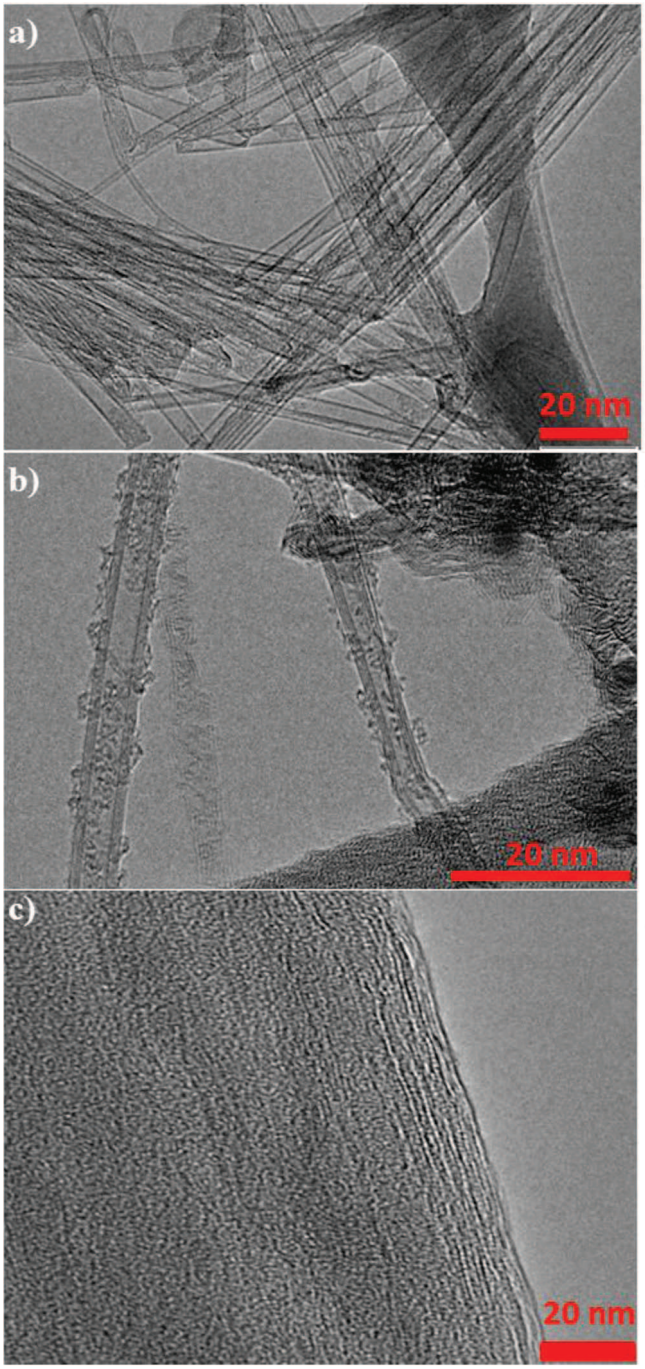

Fig. 2. TEM images of fluorinated samples; DW-300 $CF_{0.37}$ (a), FW-350 $CF_{0.37}$ (b) and CNF-405 $CF_{0.4}$ (c).

starting materials, indicating a high degree of order (Fig. 3a, b and c). The relative integrated intensities of D and G bands $\mathbf{I_D/I_G}$ are 0.22, 0.23 and 0.30 for pristine DWCNTs, FWCNTs and CNFs. It is worth mentioning that annealing treatment at high enough temperature such as the one used for FWCNTs and CNFs (1800 °C) is leading to a decrease in I_D/I_G ratio. Thus, we can assure that the structural quality of the DWCNTs sample (unprocessed) is much better than the FWCNTs.

After fluorination, the intensity of the D band increased sharply even for a low F/C of around 0.4 indicating a change of the tubes by fluorine incorporation (Fig. 4). The evolution of Raman parameters

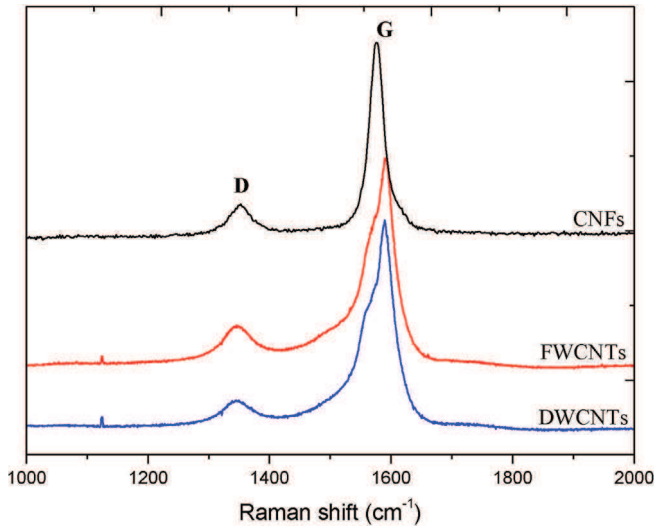

Fig. 3. Raman spectra of pristine DWCNTs, FWCNTs and CNFs starting materials. The spectra are normalized to the intensity of the band G.

shows that a low fluorination level is sufficient to significantly change the vibration modes of the carbon atoms. Fluorinated DWCNTs exhibit a $\mathbf{I_D/I_G}$ ratio of 1.00 For comparison, fully highly fluorinated graphene exhibits $\mathbf{I_D/I_G}$ of 3.8 [27]. In the case of FWCNTs, it increases up to 1.00 and for CNFs up to 1.13.

3.3. Carbon-fluorine bonding

Prior to electrochemical tests, the F/C molar ratio and the C—F bonding must be investigated because these two main parameters characterize the synthesis efficiency and then act on the electrochemical properties. In particular the theoretical capacity is calculated from the chemical composition. So ^{19}F and ^{13}C MAS NMR operating at spinning rates of 14 and 10 kHz, respectively, were carried out. The spectra are shown in Figs. 5 and 6. This technique can probe the nature of the interaction between carbon and fluorine atoms, i.e. the C—F bonding.

The ^{19}F NMR spectra (Fig. 5) show an isotropic band centered at −172, −178 and −190 ppm for fluorinated DWCNTs, FWCNTs, and CNFs, respectively, and a large number of rotational bands. This indicates that the static signal (without any rotation) is widened due to conduction electrons of the non-fluorinated inner tubes. Cobalt particles as residual catalyst may also be present in the sample. Whatever the fluorinated sample, the lines at −172, −178 and −190 ppm (Fig. 5a, b and c) are assigned to covalent C—F bonds [28–32]. It should be noted that the width of the signal is larger in the case of DW-300 compared to that of the fluorinated FWCNTs and CNFs, since the effect occurs from one tube to the other. In fact, for FWCNTs and CNFs the fluorinated tube(s) is (are) far from non-fluorinated ones and a screening effect due to the first fluorinated tube occurs. The line of covalent C—F bonds is observed at −190 ppm for fluorinated nanofibres, as for graphite fluoride (CF)n and $(C_2F)n$ structural types [28–32]. The difference in the chemical shifts for the sample is related to the curvature of the carbon lattice that results in a weakening of the covalence: the higher the curvature, the weaker the C—F bonds, the higher the chemical shift [16,22]. The values of −172, −178 and −190 ppm follow the rules for DWCNTs, FWCNTs and CNFs; the covalence increases with the diameter.

The ^{19}F line close to −120 ppm on the FW-350 and CNF-405 spectra is assigned to CF_2 groups that are not detected for DW-

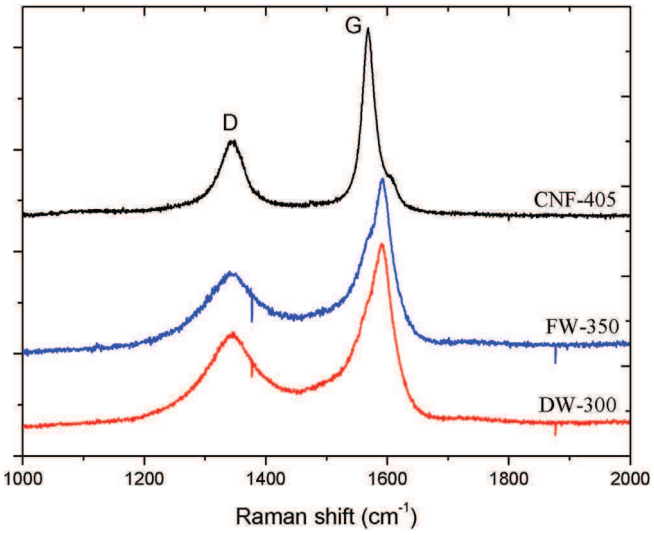

Fig. 4. Raman spectra of fluorinated nanotubes DW-300, FW-350 and CNF-405. The spectra are normalized to the intensity of the band G.

300. A small amount of CF_2 group is present for FW-350 and CNF-405 since they are prepared with F_2 gas at higher temperature compared to DWCNTs (350 and 405 °C by comparison with 300 °C, respectively). Indeed, the control of fluorination conditions avoids the hyperfluorination and fluorine covalent grafting into the carbonaceous matrix occurs without formation of important structural defects: the drastic control of the fluorination conditions allows decreasing the amount of structural defects such as CF_2, CF_3 and dangling bonds. These defects are always well correlated with structural disorder [8,13,17,33,34], and they are harmful for the electrochemical performances since these groups are insulating and prevent the lithium ionic diffusion during the discharge process [8].

The ^{13}C NMR spectra in Fig. 6, mainly show the existence of three lines attributed to three types of carbon environments: the line in the 81–84 ppm range is attributed to covalent C–F bond, and the line at 128 ppm is attributed to non-fluorinated sp^2 carbon in interaction with neighboring CF bonds along the external tube(s); The line at 120 ppm is related to the non-fluorinated carbon in the inner tube(s) without interaction with the fluorine atoms. This is a good evidence that the inner tube(s) remain(s) intact and that the fluorination concerns only the outer tube(s). It is to note that this signature of the inner tube is more visible for FW-350 while it is more difficult to locate it for DW-300 because of the presence of conduction electrons which substantially broaden the signal as discussed in the fluorine spectra.

For CNF-405, four types of nuclei are detected: i) the chemical shift at 84 ppm is characteristic of a purely covalent bond involving sp^3 hybridized carbon atoms and fluorine atoms, ii) at 42 ppm: non-fluorinated sp^3 carbon atoms in weak interaction with fluorine that are typical of a $(C_2F)n$ structure, weak interaction signifying hyperconjugation with neighboring C–F bonds, iii) at 138 ppm: non-fluorinated sp^2 carbon atoms in weak interaction with neighbors atoms of fluorine and iv) sp^2 carbon atoms without interaction with fluorine atoms (at 120 ppm as for the pure graphite). Taking into account the low fluorination level for CNF-405, i.e. $CF_{0.4}$, non-fluorinated areas are also highlighted in this sample. By combining the different information from Raman, TEM and solid state NMR, we can conclude that a similar fluorination mechanism occurs for all studied carbon nanotubes.

3.4. Electrochemical properties

Fluorinated carbon nanotubes were used as cathode material in primary lithium batteries. The 3 samples obtained by dynamic fluorination (DW-300 and FW-350 with F/C = 0.37 and CNF-405, F/C = 0.40) were tested. Samples having an intermediate F/C of about 0.3–0.4 are expected to deliver an experimental capacity that will be equal to the theoretical value in the best cases [18]. Electrochemical studies of CFx cathode materials in primary lithium batteries usually investigate samples having high F/C (in the 0.7–1 range) because of higher performances in terms of capacity [4,8,35].

The electrochemical discharge curves (at a current density of 10 mA/g) of fluorinated samples are shown in Fig. 7 with EC/PC/3DMC $LiPF_6$ 1 M as electrolyte. The initial overvoltage due to the insulating behavior of CFx with high fluorine content appears only for fluorinated CNFs. This material behaves like highly fluorinated carbons. The fluorinated outer shells are not significantly influenced by the non-fluorinated core. An opposite behavior is

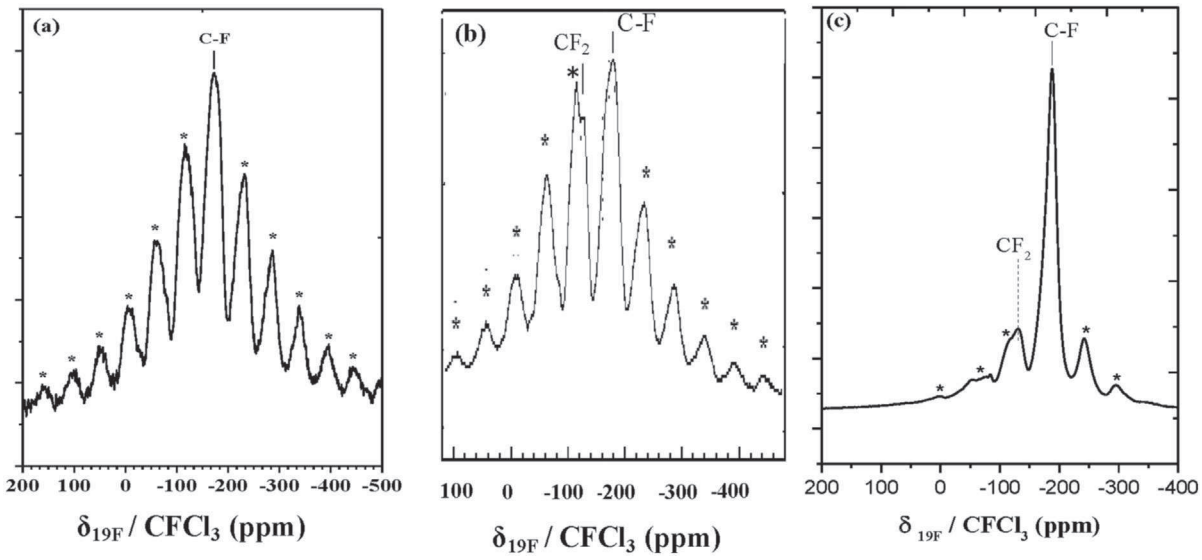

Fig. 5. ^{19}F MAS NMR spectra (14 kHz) of fluorinated DWCNTs $CF_{0.37}$ (a), fluorinated FWCNT $CF_{0.37}$ (b), CNF-405 $CF_{0.4}$ (c). (* are the spinning sidebands).

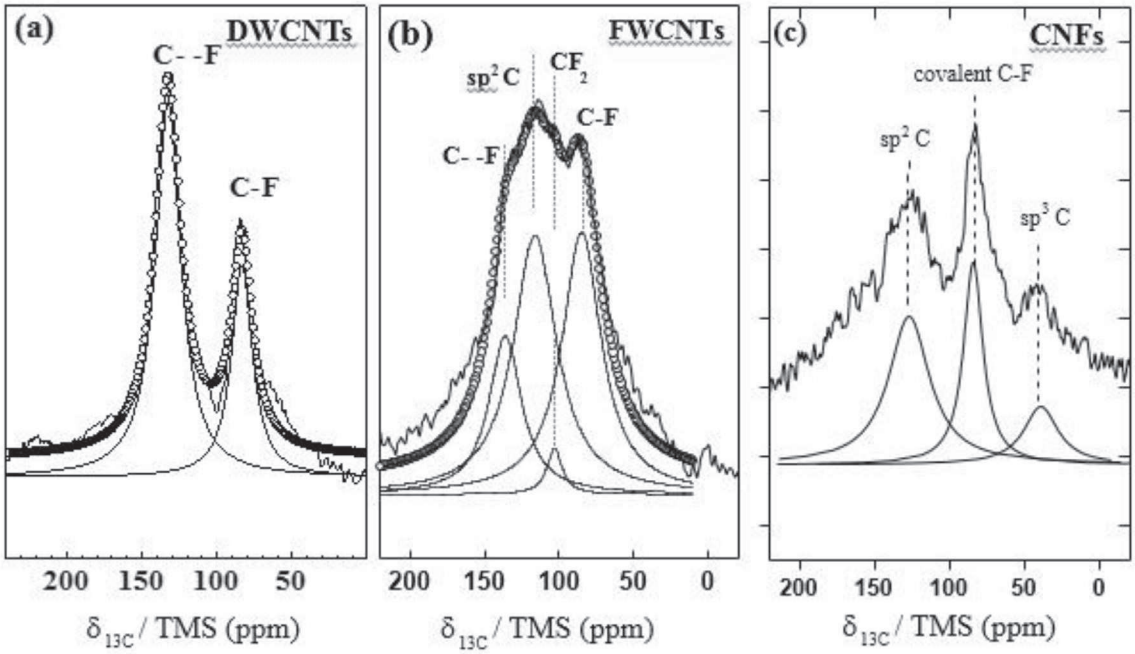

Fig. 6. ^{13}C MAS NMR spectra (10 kHz) of fluorinated DWCNTs $CF_{0.37}$ (a) fluorinated FWCNTs $CF_{0.37}$ (b) and CNF-405 $CF_{0.40}$ (c).

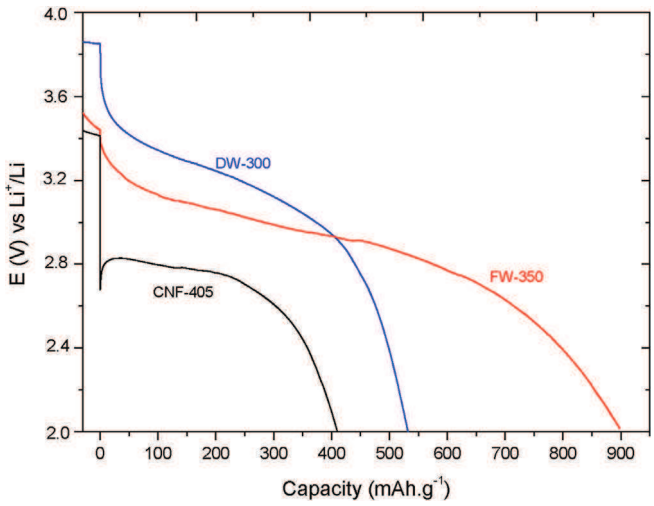

Fig. 7. Galvanostatic discharge curves obtained in EC/PC/3DMC $LiPF_6$ 1 M electrolyte at a current density of 10 mA g^{-1} for fluorinated DW-300, FW-350 and CNF-405.

observed for FW-350 and DW-300. The potential decreases continuously from the open circuit voltage. The electronic properties of the non-fluorinated inner tube allow the electron flux to be continuous. Thus, both fluorinated nanotubes keep enough electron conduction although there is 37% of fluorine into their carbonaceous matrix. It is important to note that no acetylene black was added to the formulation of the CFx cathode to ensure electronic conductivity. Taking into account the potential at half of the discharge (denoted $E_{1/2}$), the differences in the C-F covalence become obvious. The higher the covalence, i.e. the lower the curvature (large diameter), the lower the potential. $E_{1/2}$ values are 3.12 V, 2.85 V and 2.73 V for DW-300, FW-350 and CNF-405, respectively. The ^{19}F chemical shifts were −172, −178 and −190 ppm for those samples, respectively. The shapes of the galvanostatic curves also differ for fluorinated nanotubes and CNF-405. For this latter, a flat curve was recorded. The slope is more pronounced for DW-300 and, in less extent, for FW-350. This may be explained by diffusion effect of solvated Li^+ ions into the nanotubes bundles.

The most remarkable difference concerns the recorded capacities. Although a similar fluorine content was achieved in all samples (F/C = 0.37 and 0.4), significant differences in terms of capacity are evidenced.

Table 1 summarizes the electrochemical data obtained for all samples.

In particular, the experimental capacity ($\mathbf{Q}_{exp}$) significantly exceeds the theoretical value ($\mathbf{Q}_{theo}$) for FW-350 materials. Indeed, the theoretical capacity for this material is 521 mAh g^{-1} while an experimental capacity of 900 mAh g^{-1} is measured. So the faradic yield exhibit a huge value of 172% for fluorinated FWCNTs. A capacity slightly higher (531 mAh g^{-1}) that the theoretical one (521 mAh g^{-1}) was recorded for DW-300 (faradic yield of 102%) whereas CNFs exhibited only a faradic yield of 75% with a capacity of 410 mAh/g (Q_{theo} = 547 mAh g^{-1}). With similar fluorine content and amount of structural defects (with a low level), such differences may be explained by the distribution of fluorine atoms and the closeness of the non-fluorinated inner tube(s).

The discharge potential is lower for FW-350, namely 2.85 V against 3.12 V for DW-300. This difference is explained by an external diameter of the fluorinated tubes smaller for DWCNT (~2 nm estimated from TEM) [15] compared to FWCNT (~5.5 nm). The weakening of the C—F bond by the curvature effect of the carbonaceous matrix have been extensively explained [36,37]. Thanks to the extra-capacity and high discharge potential, FW-350 exhibits the highest energy density of 2565 Wh kg^{-1} for carbon fluorides used as cathode in primary lithium battery.

The highest energy density ever known for a carbon fluoride is, as far as today, of 2277 Wh kg^{-1} for low temperature graphite fluorides with hybrid C—F bonding [38] Recently, concerning nanostructured carbon fluorides, deeply fluorinated multi-walled carbon nanotubes with different diameters have shown 1923 Wh kg^{-1} energy density [39]. Thus our energy density value appears as

Table 1
Galvanostatic discharge characteristics of fluorinated samples in EC/PC/3DMC $LiPF_6$ 1 M electrolyte.

CFx	F/C	OCV (V) ±0.02	Q_{theo} (mAh/g)	Q_{exp} (mAh/g) ±20	$E_{1/2}$ (V) vs Li^+/Li ±0.02	Energy density (Wh/kg) ±80	Faradic yield (%) ±5
DW-300	0.37	3.86	521	531	3.12	1656	102
FW-350	0.37	3.62	521	900	2.85	2565	172
CNF-405	0.40	3.41	547	410	2.73	1119	75

a true overhang in primary lithium batteries.

A recent study about the electrochemical performances of another type of carbonaceous materials (a mixture of nanodiscs/nanocones 20/80 w.%) [13] evidenced similar phenomenon of extra-capacity [13] which is at the origin of our high energy density. This 2D lattice was fluorinated by atomic fluorine released by thermal decomposition of solid fluorinating agent TbF_4 resulting in very few structural defects and an homogenous dispersion of fluorine atoms into the outer discs; the central disk(s) remained less or not fluorinated [8,13,17,18,37]. Note also that in the case of fluorinated carbon nanofibers (CNFs), extra-capacity has never been obtained neither with the controlled nor with the dynamic fluorination and a faradic yield of about 88% (for controlled process) and 77% (for direct one) were measured [8,13,40]. In other terms, the physico−chemical characteristics obtained with the controlled process (i.e. few defects and homogenous dispersion of fluorine atoms) are necessary for this kind of carbonaceous 2D materials [13]. It was concluded that the reinforcement effect of the non-fluorinated central discs, coupled with a low amount of structural defects CF_2, CF_3, is a key parameter to achieve the extra-capacity. This reinforcement effect allows the rebuilding of the carbon lattice during the electrochemical de-fluorination and then different sites of insertion of Li^+ species are possible in the reconstructed carbon lattice [13]. Furthermore, the presence of a shell of LiF seems to allow the diffusion of the lithium ions (either Li^+ of Li_2F^+) through the sheet edges or the surface cracks (disruptions of the sheets); thus insertion may be an additional phenomenon after the electrochemical de-fluorination, resulting in the extra-capacities [13].

To go further on the similitudes between fluorinated FWCNTs and nanodiscs, i.e. the two first examples of extra-capacities, the location of LiF particles was investigated with TEM. TEM images of the DW-300 and FW-350 composite electrode after full discharge are shown in Fig. 8.

After full discharge, nanotubes are still observed and are covered by a thick layer. In agreement with the well-known mechanism of formation of LiF with the reduction of CF_x [8,12,13,41], these particles can be attributed to LiF. By analogy to lithium-graphite intercalation compounds, such as LiC_6, F^- ions, which are formed during the fluorocarbon reduction, diffuse within the interlayer and combine with solvated Li^+ on the sheet's edges [42,43]. A recent study on the discharge mechanism of fluorinated carbon nanofibres showed that such particles made of LiF, are formed outside the carbonaceous matrix [8,13]. After the full discharge, the fluorocarbon matrix is totally converted into carbon. LiF peaks are observed at 39°, 45° and 65° in 2θ values (powder XRD analysis not show here). The formation of crystalline LiF particles is emphasized by the sharpness of the peaks [8,13]. It is to note that the discharge mechanism is nearly similar regardless the nanocarbon used, discs, tubes or fibers [8,13].

By analogy with what has been explained above, the high faradic yield obtained for FW-350 is due to an additional electrochemical process similar to insertion of lithiated species. Different lithium insertion sites may be active: i) between initial non-fluorinated tubes which act as reinforcement tubes and the reconstructed carbon by the electrochemical defluorination, ii) between the tubes in the bundles.

Considering that unfluorinated carbon and electrochemically defluorinated carbon can insert lithium following the ratio 1 lithium for 6 carbon as in graphite intercalation compound, it is an extracapacity of 372 mAh/g that can be added to the electrochemical reduction of carbon fluorides. In the case of FW-350, our prediction should lead to a theoretical capacity of 893 mAh/g which is almost the same value than the experimental value obtained more or less the uncertainties of measure.

The extra-capacity was mainly obtained with FW-350 material (faradaic yields of 172%). No extra-capacity was obtained with CNF-405 (faradic yield of 75%) (Table 1). With DW-300, we can suspect some extra-capacity having in mind that classical faradic yields for graphite fluoride used in primary lithium battery is around 80% [2]. All the results are a formal indication that extra-capacity depends on the number of concentric tubes, and also there is an optimal number of tubes to obtain extra-capacity. Too many tubes (the case of CNF) are not favorable for extra-capacity. For CNFs external fluorinated shells are insensitive to the non-fluorinated core, at least for a F/C ratio of 0.4 in our experimental conditions.

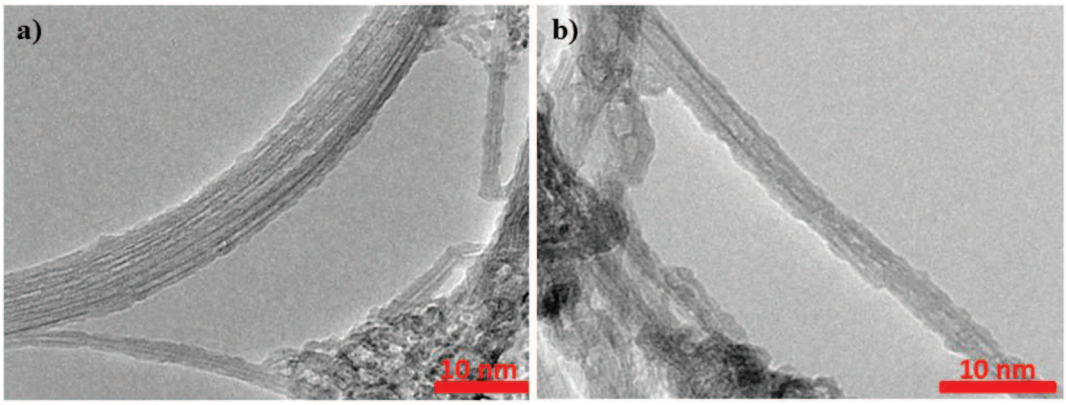

Fig. 8. TEM images of DW-300 a) and FW-350 b) composite electrode after full discharges.

Moreover, the amount of LiF plays a key role, it is too small for DW-300 and as a consequence not sufficient to make a huge second electrochemical process. The difference can be also explained by a greater reinforcement effect for FWCNT due to the presence of more number of tubes that provides this reinforcement and reformed carbon able for insertion. Thus, the lithium insertion sites are more efficient through LiF coating (as for nanodiscs) for FWCNT than for DWCNT. Such a process can occur through the LiF layer on the nanotubes, thicker in the case of FWCNT. Thus, the lithium insertion sites are much more likely for FWCNT than for the DWCNT. Once again, such a process may occur through the layer of LiF as a coating on the nanotubes, this layer allowing the exchange of lithiated ions with the electrolyte.

4. Conclusions

The present work has the originality to invest fluorinated materials with relatively low fluorine content (F/C = 0.37) and shows that a low amount of fluorine is not detrimental to achieve excellent electrochemical performances. The combination of extra-capacity (900 mAh/g), even with a low fluorination level, and a high discharge potential (2.85 V) leads to an exceptional energy density of 2565 Wh/kg for sub-fluorinated FWCNTs. This has an industrial interest since the synthesis cost will be lowered without affecting the electrochemical performances. Both fluorine consumption and fluorination temperature are decreased resulting in lower costs that are the main drawback of fluorinated carbons as cathode in primary lithium battery.

In this work, extra-capacities are obtained with fluorinated nanotubes (1D) by the direct fluorination with F_2 gas. Thus, for a closed structure such as carbon nanotubes (1D, tubular) dynamic fluorination appears to be the most convenient way, whereas for opened structure such as carbon nanodiscs/nanocones (2D in majority, discotic), controlled fluorination with atomic fluorine is a better strategy. The concept of reinforcement to reach extra-capacity may be probably expanded to other carbonaceous nanomaterial keeping in mind the strong effect of the nanomaterial nature, its morphology, shape factor, the stacking of the graphene layers (in tubes or sheets), etc. Fluorination route, as well the fluorine content, must be adapted/optimized in each case.

Acknowledgements

The authors want to thank Elodie Petit for Raman analysis and Pierre Bonnet for his contribution for TEM measurements.

References

[1] M. Fukuda, T. Ijima, in: Proc. of 9th Internationnal Power Sources Symposium, 1974, p. 713. London.
[2] N. Watanabe, M. Fukuda. US Patent 3 536 532, 1970 and 3 700 502, 1972.
[3] A. Hamwi, K. Guérin, M. Dubois. Chapter 17. Elsevier, Oxford, UK, (2005).
[4] R. Yazami, A. Hamwi, K. Guérin, Y. Ozawa, M. Dubois, J. Giraudet, F. Masin, Electrochem. Commun. 9 (2007) 1850–1855.
[5] R. Yazami, A. Hamwi. WO2007098478 (2007), WO2007126436(2007) and EP1999812 (2008), EP1976792 (2008).
[6] H.J. Yue, W. Zhang, H.D. Liu, Z.G. Liu, G.M. Zhong, Y. Yang, Nanotechnology 24 (2013) 424003.
[7] H. Groult, C.M. Julien, A. Bahloul, S. Leclerc, E. Briot, A. Mauger, Electrochem. Commun. 13 (2011) 1074–1076.
[8] Y. Ahmad, K. Guérin, M. Dubois, W. Zhang, A. Hamwi, Electrochim. Acta 114 (2013) 142–151.
[9] J. Giraudet, C. Delabarre, K. Guérin, M. Dubois, F. Masin, A. Hamwi, J. Power Sources 158 (2006) 1365–1372.
[10] M.S. Whittingham, J. Electrochem. Soc. 122 (1975) 526.
[11] K.M. Abraham, D.M. Pasquariello, in: The Electrochemical Society Proceedings, 1991. PV91–3.
[12] S.S. Zhang, D. Foster, J. Wolfenstine, J. Read, J. Power Sources 187 (2009) 233–237.
[13] Y. Ahmad, M. Dubois, K. Guérin, A. Hamwi, W. Zhang, Carbon 94 (2015) 1061–1070.
[14] E. Flahaut, R. Bacsa, A. Peigney, C. Laurent, Chem. Commun. (2003) 1442–1443.
[15] E. Flahaut, C. Laurent, A. Peigney, Carbon 43 (2005) 375–383.
[16] W. Zhang, M. Dubois, K. Guerin, P. Bonnet, H. Kharbache, F. Masin, A.P. Kharitonov, A. Hamwi, Phys. Chem. Chem. Phys. 12 (2010) 1388–1398.
[17] Y. Ahmad, E. Disa, M. Dubois, K. Guérin, V. Dubois, W. Zhang, P. Bonnet, F. Masin, L. Vidal, D.A. Ivanov, A. Hamwi, Carbon 50 (2012) 3897–3908.
[18] Y. Ahmad, E. Disa, K. Guérin, M. Dubois, E. Petit, A. Hamwi, P. Thomas, J.L. Mansot, J. Fluor. Chem. 168 (2014) 163–172.
[19] F. Chamssedine, M. Dubois, K. Guérin, J. Giraudet, F. Masin, D.A. Ivanov, L. Vidal, R. Yazami, A. Hamwi, Chem. Mater. 19 (2006) 161–172.
[20] A. Hamwi, H. Alvergnat, S. Bonnamy, F. Béguin, Carbon 35 (1997) 723–728.
[21] R. Yazami, A. Hamwi. PCT/US06/60991, (2006).
[22] M. Dubois, K. Guérin, W. Zhang, Y. Ahmad, A. Hamwi, Z. Fawal, H. Kharbache, F. Masin, Electrochim. Acta 59 (2012) 485–491.
[23] A.C. Ferrari, Solid State Commun. 143 (2007) 47–57.
[24] A.C. Ferrari, J.C. Meyer, V. Scardaci, C. Casiraghi, M. Lazzeri, F. Mauri, S. Piscanec, D. Jiang, K.S. Novoselov, S. Roth, A.K. Geim, Phys. Rev. Lett. 97 (2006) 187401.
[25] A.C. Ferrari, J. Robertson, Phys. Rev. B 61 (2000) 14095–14107.
[26] Z. Wang, X. Huang, R. Xue, L. Chen, J. Appl. Phys. 84 (1998) 227–231.
[27] F. Withers, M. Dubois, A.K. Savchenko, Phys. Rev. B 82 (2010) 073403.
[28] A.M. Panich, Synth. Met. 100 (1999) 169–185.
[29] M. Dubois, J. Giraudet, K. Guérin, A. Hamwi, Z. Fawal, P. Pirotte, F. Masin, J. Phys. Chem. B 110 (2006) 11800–11808.
[30] J. Giraudet, M. Dubois, K. Guérin, C. Delabarre, A. Hamwi, F. Masin, J. Phys. Chem. B 111 (2007) 14143–14151.
[31] J. Giraudet, M. Dubois, A. Hamwi, W.E.E. Stone, P. Pirotte, F. Masin, J. Phys. Chem. B 109 (2004) 175–181.
[32] T. Mallouk, B.L. Hawkins, M.P. Conrad, K. Zilm, G.E. Maciel, N. Bartlett, Philos. Trans. Roy. Soc. A 314 (1985) 179–187.
[33] M. Dubois, K. Guérin, J.P. Pinheiro, Z. Fawal, F. Masin, A. Hamwi, Carbon 42 (2004) 1931–1940.
[34] K. Guérin, J.P. Pinheiro, M. Dubois, Z. Fawal, F. Masin, R. Yazami, A. Hamwi, Chem. Mat. 16 (2004) 1786–1792.
[35] K. Guérin, M. Dubois, A. Houdayer, A. Hamwi, J. Fluor. Chem. 134 (2012) 11–17.
[36] J. Giraudet, M. Dubois, K. Guérin, J.P. Pinheiro, A. Hamwi, W.E.E. Stone, P. Pirotte, F. Masin, J. Solid State Chem. 118 (2005) 1262–1268.
[37] M. Dubois, K. Guerin, W. Zhang, Y. Ahmad, A. Hamwi, Z. Fawal, H. Kharbache, F. Masin, Electrochim. Acta 59 (2012) 485–491.
[38] K. Guérin, R. Yazami, A. Hamwi, Electrochem. Solid St. 7 (2004) A159–A162.
[39] Y. Li, Y. Feng, W. Feng, Electrochim. Acta 107 (2013) 343–349.
[40] W. Zhang, K. Guérin, M. Dubois, Z.E. Fawal, D.A. Ivanov, L. Vidal, A. Hamwi, Carbon 46 (2008) 1010–1016.
[41] E. Rangasamy, J. Li, G. Sahu, N. Dudney, C. Liang, J. Am. Chem. Soc. 136 (2014) 6874–6877.
[42] A. Naji, P. Willmann, D. Billaud, Carbon 36 (1998) 1347–1352.
[43] J. Giraudet, M. Dubois, J. Inacio, A. Hamwi, Carbon 41 (2003) 453–463.